Piecewise-focusing collectors reduce the mirror area in concentrating solar thermal power plants

David K Bisset
Research Engineer
Canberra ACT Australia
Email: davidkbisset@gmail.com

ABSTRACT

Piecewise-focusing (PWF) collectors replace the heliostat field and central tower receiver of Gen 2 concentrating solar thermal (CST) power plants. The PWF collector consists of a large base frame supporting a tiered array of reflectors that concentrate sunlight into a cavity receiver. The base frame rotates about a central pivot to track the sun in azimuth, while the reflectors rotate about individual nearly-horizontal inclined axes to track the sun in elevation. Compressed gas such as CO_2 is used as the heat transfer fluid (HTF) from the receiver to a conventional molten salt thermal reservoir, which supplies heat for a steam turbine power block. Physical and numerical modelling of an approximately paraboloidal PWF collector shows that about 250 separate reflectors will be required for adequate focus on the entrance to a cavity receiver at concentration ratio 2000 with little spillage at all sun elevations. With an area 10-20 times larger than the cavity entrance, the absorber functions at peak temperatures that are within range of standard stainless steel tubing, despite using a gaseous HTF. Reflectors of PWF collectors have significantly better cosine factors than heliostats, and cavity receivers lose much less heat than open cylindrical receivers, so that reflector area is reduced to about 62% of heliostat area. Thus the capital cost of a CST plant can be reduced substantially. By continuing to use Gen 2 technology for thermal storage and the power block, PWF-based CST can be developed much sooner than 'Gen 3' CST.

1 Introduction

The main advantage of concentrating solar thermal (CST) power plants over many other forms of renewable energy is that collected energy can be stored quite cheaply and very efficiently for many hours in the form of heat, and then converted to electricity when demand is high and/or the sun has set. The first generation of CST power plants with storage mainly utilized line-focus parabolic trough collectors, indirectly-heated molten 'solar salt' for thermal storage, and a steam-Rankine cycle power block [1]. An example is the 250 MW Solana Generating Station in Arizona, USA [2]. Generation 2 CST power plants, i.e. central receiver or 'power tower' systems, utilize point-focus designs with the molten salt heated directly in a

receiver illuminated by heliostats [1]. The result is higher temperatures and thus higher efficiency for both thermal storage and the power block. The Noor III power plant in Morocco, producing 134 MW for seven hours after sunset, is an example of this type [3].

For Generation 3 of CST [1] it is envisaged that a heliostat field with some type of central receiver will still be used, but the power block will operate on a modified Brayton cycle with supercritical CO_2 (sCO_2) as the working fluid at higher temperatures than possible with current steam technology, aiming for yet higher efficiency. Notional thermal efficiencies for just the power blocks are 33% (first generation), 43% (Gen 2), and at least 50% (Gen 3). However, Gen 3 temperatures are too high for using 'solar salt' as heat transfer fluid (HTF) and/or for thermal storage, and therefore both the storage system and the collector that supplies it will have to be redeveloped along with the new power block (heliostat fields will not change greatly). For example, solid particle receivers and storage are under development [4, 5], along with particle-to-sCO_2 heat exchangers [6]. The *Gen 3 Roadmap* of 2017 [1] indicated that it could take ten years to develop the first Gen 3 demonstration plant; commercial applications would take even longer. Also, collector efficiency tends to decrease as power block input temperature increases. Dunham and Iverson [7] showed that the combined efficiency of receiver and power block actually decreases above a certain input temperature. Under certain assumed conditions, a directly-illuminated sCO_2 receiver and power block combined efficiency peaks at 39.1% (turbine inlet temperature 766 C). With similar assumptions the Gen 2 combined efficiency at 565 C is about 38% ([7], and therefore the benefits from the sCO_2-Brayton cycle might be fairly limited. If greater heliostat aiming precision is required to achieve the higher receiver temperature, the cost of the plant may well be greater. None of the changes from Gen 2 to Gen 3 can equal the earlier change from line-focus to point-focus in its impact.

The thesis of the present work is that by using Piecewise-Focusing (PWF) collectors instead of heliostats and a central receiver, existing Gen 2 technology can be developed quite quickly into CST power plants with storage that are more efficient, more cost-effective, and more flexible in design and operation, than existing 'power tower' plants, as follows: (1) The steam Rankine-cycle power block is essentially unchanged. (2) Receiver operation and thermal storage in 'solar salt' are simplified by heating the salt indirectly, using a compressed gas HTF in the receivers instead of the molten salt itself. (3) The central receiver (daily average thermal efficiency around 85%) is replaced by several cavity receivers (efficiency over 96%). (4) The sunlight-concentrating function of the heliostat field (average reflection efficiency[1] about 60%) is performed by the PWF reflectors (average reflection efficiency around 85%). This paper concentrates on numerical and physical modelling of PWF designs, and analyzes the absorber area of compressed-gas cavity receivers. It is assumed throughout that a suitable geometrical concentration ratio (CR) from the PWF reflectors into the cavity receiver entrances is 2000.

2 Heliostats and separation of scales for sun-tracking

The concept of multiple overlapping reflections of the sun producing high temperatures was suggested by Archimedes as a means of repelling Roman ships invading Syracuse in 212 BCE. Legend has it that soldiers stood around the shoreline and aimed reflections from highly-polished shields, thus becoming precursors of the heliostat: a reflector with fixed position and variable orientation, capable of reflecting sunlight continuously to a target in a fixed direction. However, the earliest use of an array of heliostats as a solar collector to produce heat for conversion to mechanical power (as distinct from the

[1] Reflection efficiency = (sunlight flux reaching receiver aperture) / (DNI * gross mirror area)

paraboloidal dish or parabolic trough) is generally attributed (by Falcone [8] among others) to work carried out in the Soviet Union in the early 1950s. In particular, the work of Baum et al [9] published in 1957 is often referenced, e.g. by Li et al [10]. The modern central receiver or 'power tower' designs — an array of heliostats surrounding a tower-mounted receiver — are conceptually very similar to a 1949 design by N.V. Lenitski that was described by Baum et al [9]. However the latter group rejected that design on the grounds that the tower would be too tall in an installation of sufficient power. Instead, for their main analysis and experiments, they introduced two new ideas, as follows.

2.1 The moving field

Baum et al [9] replaced the heliostat array with a 'moving field' of 15 m^2 tilting reflectors mounted on railway wagons, which rotated around the central boiler tower on 23 concentric tracks to follow the azimuthal position of the sun. Because they move, these reflectors are not strictly heliostats, although they can be regarded as heliostats with respect to axes rotating with the field. An advantage of azimuthal movement of the entire field is that the reflectors face the sun more squarely over the course of a day, reducing cosine losses and increasing the daily energy collection per m^2 of mirror.

2.2 Separation of scales for sun-tracking axes, with single-axis mounting of reflectors

Baum et al [9] determined that each reflector could be rotated about a single inclined axis for mounting on its wagon, a great simplification compared to the two-axis rotation required for heliostats. Effectively the scales of rotation are separated for tracking the sun in azimuth and elevation: largest-scale rotation (the entire field) for azimuthal tracking, and smallest-scale rotation (the individual reflector) for elevation. Conventional heliostats require up to 90° of rotation in elevation and must track the sun as it moves through up to 270° in azimuth, which is usually accomplished with precision gear drives, but the Baum-style reflector needs about 45° of rotation in elevation only, with simple linear actuation possible. Movement of the wagons around their tracks with equal angular velocity is also required, but the cost of doing so is counterbalanced by the savings in single-axis elevation tracking. The orientation of the inclined mounting axis for each reflector depends on its position in the moving field, as does the angle between the reflector and its mounting axis. With this mounting scheme, the aim of the reflector towards the receiver varies slightly with sun elevation and is only perfect at three arbitrarily-chosen elevations, but aiming errors at other elevations are small, less than 1'15" (0.36 mrad) for the conditions analyzed by Baum et al [9]. A 1:50 scale model of part of the proposed design was constructed [9]. To the author's knowledge, no subsequent moving-field design (apart from the present proposal) adopted the single-inclined-axis mounting scheme for reflectors.

Various other designs of moving field collectors were proposed subsequently. For example, Jones [11] designed a platform supported on a large number of rollers to replace the railway wagons, optionally running on an amphitheater-like embankment. Ruiz et al [12] constructed a version with trolleys that support large conventional heliostats on several concentric tracks at the CTAER in Spain. However, the direct benefit of a moving field is only modest — Ruiz et al [12] found that annual heat collection increased by 8-10% for a certain polar-type heliostat layout — and it is debatable whether this justifies the increased cost and complication if dual-axis reflectors are still used. Similarly, the Jones [11] design was not adopted when compared with standard heliostats in a 2007 cost reduction study [13]. As for a conventional heliostat field, the reflectors in a large moving field at ground level must be widely spaced in order to reduce mutual shading and blocking.

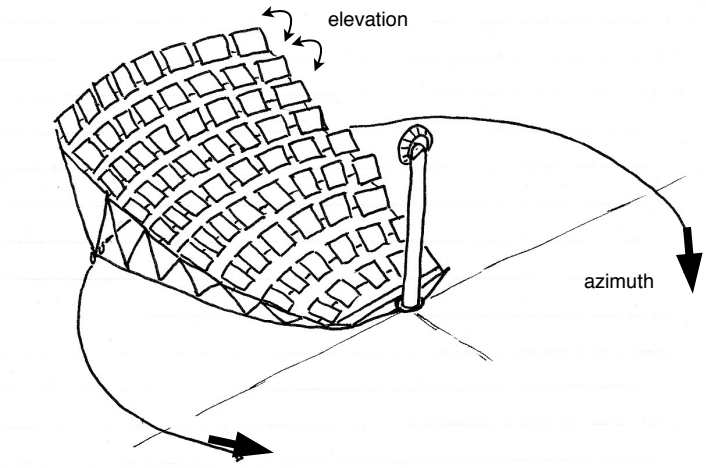

Fig. 1. Concept sketch of a PWF collector [14]. The entire collector tracks the sun in azimuth. Each reflector (mirror unit) tracks sun elevation independently by rotating about a fixed inclined axis.

3 The piecewise-focusing collector

The piecewise-focusing (PWF) collector was conceived as a large collector divided into independent reflectors, as sketched in Fig. 1, with separation of scales for the rotational axes. A lightweight base-frame provides azimuthal motion and supports a tiered array of a hundred or more slightly curved reflectors, each mounted on its own single, nearly-horizontal inclined axis that allows sun-tracking in elevation. Compared to a moving field at ground level, the tiered PWF collector allows much closer spacing of the reflectors, which can cover a high percentage of the gross aperture area with little shading or blocking. However, the largest practicable size for a PWF collector is likely to be smaller than could be achieved with a ground-level moving field. The concept of using a single inclined axis for each reflector was developed independently by the present author [14], and the method for determining axis inclinations is slightly different from that of Baum et al [9], but the results appear to be equivalent.

3.1 Determination of reflector-axis mounting angles

Each reflector (mirror unit) rotates about a single axis fixed to the base frame. For a given reflector, vector **a**, the direction of its axis relative to the base frame, and the angle α between the axis and the plane tangent to the center of the reflector (Fig. 2), are to be determined. Note that all vectors in the following are of unit length, and therefore only two components of **a** are independent — there are three unknowns including α.

Coordinate axes are fixed to the base frame at the center of the given reflector. Let **r** and $\mathbf{r}''$ be respectively the directions from sun to reflector and from reflector to receiver (Fig. 2); $\mathbf{r}''$ is fixed, and because of the base frame's azimuthal rotation **r** depends only on sun elevation. Let **n** be the inwards normal to the reflector; then for specular reflection it is required that

$$\mathbf{n} = \frac{\mathbf{r} - \mathbf{r}''}{|\mathbf{r} - \mathbf{r}''|} \tag{1}$$

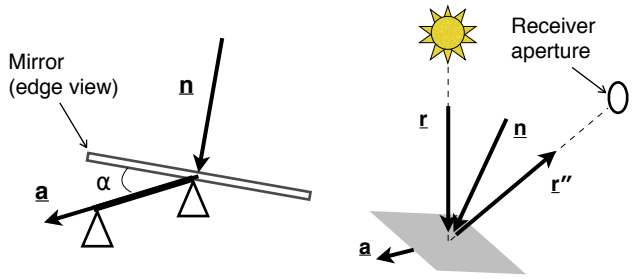

Fig. 2. Definition sketches for Section 3.1. The reflector (mirror) tilts around an axis (direction $\mathbf{a}$) fixed to the base frame, and is set at angle α to that axis. Vector $\mathbf{r}''$ is fixed by the particular reflector's position in the array of reflectors, and $\mathbf{r}$ depends only on sun elevation.

Also, since α is fixed for a given reflector,

$$\mathbf{n} \cdot \mathbf{a} = \cos(\pi/2 - \alpha) = C \tag{2}$$

where C is a constant, or,

$$\mathbf{n} \cdot (\mathbf{a}/C) = 1 \tag{3}$$

Select three values of sun elevation, giving three numerically different versions of this equation, and solve simultaneously for the three Cartesian components of $(\mathbf{a}/C)$. Finally,

$$\alpha = \pi/2 - \arccos C \tag{4}$$

The result is a reflector with perfect aim from its center at any three chosen sun elevations, and small aiming errors at other elevations.

3.2 The 'segmented dish' as an example PWF collector

In terms of optical performance, the ideal model for a PWF collector is a paraboloidal dish at a fixed angle of tilt, divided into reflectors that cover nearly 100% of the putative dish surface. However, other shapes may be more practical for economical construction, and require only small increases in the spacing between reflectors to avoid shading and blocking.

The following analysis assumes a 'segmented dish' as shown in Fig. 3. It is based on a paraboloidal surface that has a rim angle of 22.5° (the cone of light reflected to the focus has a vertex angle of 90°), and a fixed tilt towards the sun of 30°. The surface is divided into 80 slightly curved rectangular reflectors, each fixed at a specific angle to its axis of rotation, and that axis is mounted at a specific angle to the base frame (determined as above). Each reflector is controlled by its own independent tilting mechanism (for example, a linear actuator). A planar target, normal to the segmented dish axis and representing the entrance to a cavity receiver, is fixed at the focus. Figure 4 shows a simplified 3D model of the right-hand half of the segmented dish using a smaller number of larger reflectors, with the latter tilted as required at three different sun

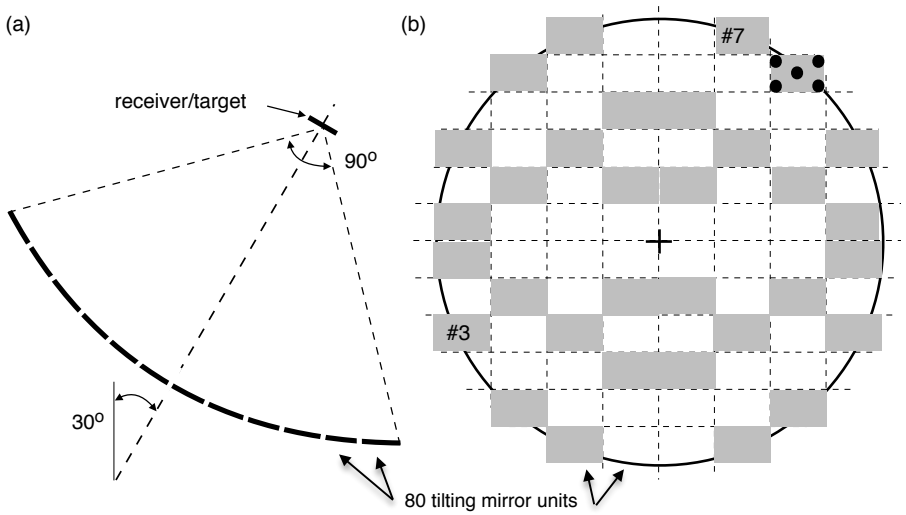

Fig. 3. The segmented dish. (a) Side view cross-section. (b) View into the aperture. Grey: reflectors used in the numerical model. Dots: reflector for the scaled-up model in Sec. 4. Numbers: reflectors used for the results in Fig. 5.

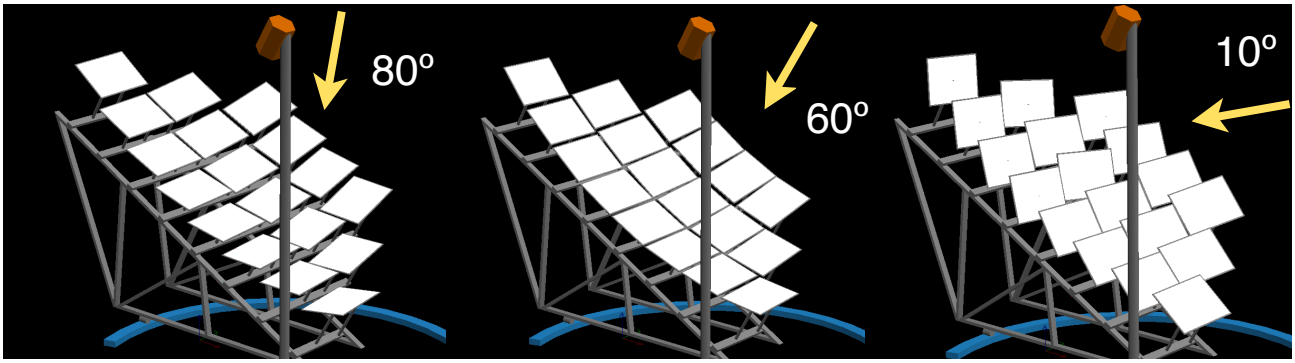

Fig. 4. Simplified 3D model of the segmented dish using oversized reflectors; only right-hand half shown for clarity. Reflectors are tilted as required at the three sun elevations indicated.

elevations. The base frame and axis mountings are very stylized in Fig. 4, but the mounting angles and angles of tilt are approximately correct for each reflector. It may be inferred that mutual shading between reflectors is not significant unless the sun is near the horizon.

Numerical models for 32 out of the 80 reflectors (Fig. 3) were set up [14, 15], modelling the reflectors indicated in Fig. 3(b). A physical model of 3.6 m aperture diameter incorporating 10 of those reflectors was constructed [14], and was used to explore PWF ideas and qualitatively verify numerical results. Since the reflectors are large enough to cause astigmatism of their reflected light as the sun elevation varies, a more accurate, larger-scale model of one reflector was constructed [15] for quantitative comparison with the numerical model, particularly at the corners of the rectangular reflector. Astigmatism results are given in Secs. 4 and 5, but an idea of mirror unit mounting angles can be had from the photographs (Fig. 6) of the larger-scale physical model.

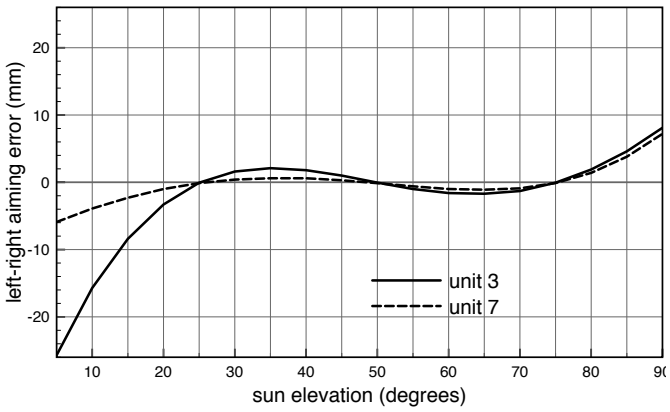

Fig. 5. Left-right aiming errors on the target from the centers of two reflectors (mirror units). Adapted from [14].

3.3 Testing mirror aim

Aiming errors from the centers of several reflectors were examined in the independent numerical model. For a given sun elevation, a specified reflector is rotated about its axis by very small steps in the model until the aiming error of its reflected ray reaches a minimum, which is reported in milliradians. Then the reflected ray is intersected with the target plane and the 2D error on the target is reported in millimetres. Since reflector axes are nearly horizontal, the reflected image on the target moves nearly vertically when a reflector is rotated, so vertical aiming errors can be made very small. Therefore the main aiming errors on the target are horizontal (i.e. left-right).

Figure 5 shows left-right aiming errors as a function of sun elevation for the two reflectors (mirror units) indicated in Fig. 3(b), using sun elevations of (25°,50°,75°) for determining axis mounting angles. As expected, the errors are essentially zero at these elevations. They are quite small between these elevations, and increasing rapidly (for Unit 3 at least) when the sun is near the horizon. Note that 3 mm = 1 milliradian approximately (varies somewhat for different reflectors). Broadening the spread of sun elevations for finding axis angles results in better aim at low sun elevations with little penalty elsewhere [14], and it was also shown in that paper that small construction errors in reflector mounting would not distort reflector aim unacceptably.

4 Aiming errors from the corners of a reflector

As noted earlier, the relatively large size of reflectors is potentially a problem for collector focus at different sun elevations. Aims from the corners of a reflector deviate much more than the aim from its center, causing astigmatism and possibly spillage at low and high sun elevations. The PWF segmented dish used for this work (Fig. 3) has only 80 reflectors covering its aperture, whereas the moving field designs mentioned earlier contain much larger numbers of relatively smaller reflectors: 624 [12], 1293 [9], or 2200 [11]. Before the numerical model was used to investigate astigmatism, it was tested against a physical model of the reflector indicated by five dots in Fig. 3(b), scaled up so that the notional aperture diameter of the segmented dish would be 6.0 m instead of 3.6 m. The reflector chosen is at the edge of the aperture in one of the areas where axis inclinations are largest — i.e. it is a ‘worst case’ position.

Views of the 750 x 500 mm model reflector are shown in Fig. 6, along with a sample of reflections onto the target. This figure gives an idea of how the reflector axis is turned counterclockwise (in this case) in the horizontal plane, and of how the

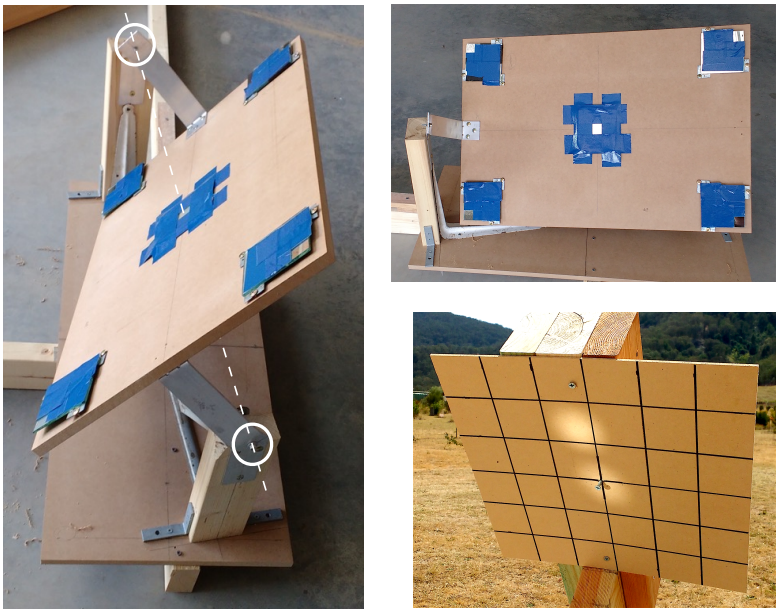

Fig. 6. The scaled-up model reflector, and sample reflections on the target from its center and one corner. Mirror tiles are masked to permit reflections from only the center and corners of the unit. The inclined axis of rotation for tracking sun elevation is indicated by the dashed line (left) through the two pivot points (circles). Adapted from [15].

mirror tangent plane is set at a considerable angle (25.3° in this case) to its mounting axis (white dashed line). The axis was determined using sun elevations of (15°,45°,75°). The reflector was equipped with 100 x 100 mm mirror tiles at its center and corners, masked down to 25 x 25 mm.

Corner tile aims were set to coincide with the center when the sun was at 45° elevation. An example of reflections on the target (which has a 50 mm square grid) from the center tile and one corner is given in Fig. 6 (sun elevation $\neq 45°$). It can be seen that each patch of light spreads considerably because of the finite size of the sun, and therefore it is difficult to assess the position of each patch with precision better than about 10 mm.

Numerical and physical results for corner ray intersections with the target are compared in Fig. 7. Numerical results are given from sun elevations 10° to 80° at 10° intervals; physical results are given at various elevations between the endpoints shown. An unquantifiable amount of slack was present in the mirror tile aim adjustment screws, which combined with the imprecision in picking the center of each patch of light on the target to add a bit of randomness to the results. Nevertheless, the overall agreement between physical and numerical results is sufficient to give confidence in the numerical modelling that follows.

5 Images formed on the target plane

The 32 reflectors colored grey in Fig. 3(b) were added to the numerical model, and intersection points on the target plane were calculated for the centers and corners of all 32 reflectors. As for the single reflector above, the PWF collector aperture diameter was 6000 mm, reflector axes were determined using sun elevations of (15°,45°,75°) and the corner aims were set with the sun at 45°. In Fig. 8 the intersection points are combined into images (focus maps) on the target plane that

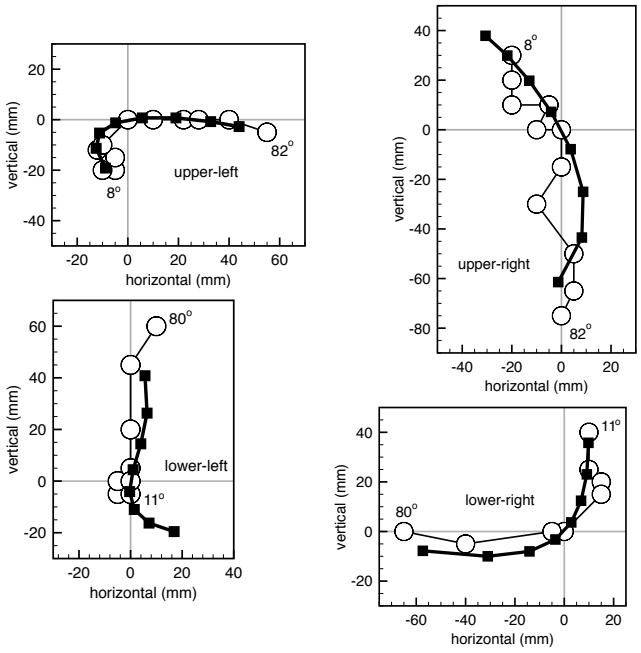

Fig. 7. Comparison of results from the scaled-up reflector and its numerical model. Physical (circles) and numerical (squares) intersection positions on the target from corner rays as a function of sun elevation. Adapted from [15].

represents the entrance to a cavity receiver, at a range of sun elevations from 10° to 80° above the horizon. Each intersection of a reflected ray with the target is indicated by a dot, but in practice the finite size of the sun would blur that dot by 15-20 mm in all directions. The larger circle indicates a nominal concentration ratio (CR) of 2000, and the smaller (dashed) circle allows for blurring caused by the finite size of the sun. Localised slope errors on the mirror surfaces are not accounted for, but on the other hand the points on the figures come from the extreme corners of the reflectors and reflected light from the remainder of each reflector is better aimed. Note that although the variation in effective concentration at the cavity entrance is quite large, the light rays arrive in a cone shape with a 90° vertex angle and fan out similarly inside the cavity receiver. The vertex of the cone becomes sharper at intermediate sun elevations but the effect on the cavity interior walls is quite small.

Figure 8 shows that collector focus is very satisfactory for sun elevations between about 30° and 70°, but focus at 20° is borderline and at 10° unacceptable. The focus at 80° is also borderline, but outside the tropics this elevation is only reached around noon near the summer solstice (if at all). Results at low elevations can be improved at the design stage by (a) increasing the tilt angle of the collector axis, currently 30° (Fig. 3a), (b) decreasing the sun elevation at which the reflector corners are aimed perfectly (currently 45°), and/or by (c) deleting the offending reflectors (mainly at the very bottom of the collector aperture); also those reflectors could be turned off-sun during daily startup and shutdown. Note that the first two options degrade the results at high sun elevations. Another option is to reduce the size of reflectors (all of them, or just the problem cases) relative to the collector, with a corresponding increase in their number, and their shape can be changed too (currently a 3:2 rectangle). It was shown in [15] that division of the aperture into 200 to 320 equal-size reflectors would be sufficient at all sun elevations for a nominal CR of 2000, with a roughly square shape preferable. Hexagonal reflectors also give good results. This analysis applies to the 'segmented dish' of geometry shown in Fig. 3, and it would have to be re-done for any other tiered shape of PWF collector. Also, the practicalities of manufacturing the reflectors must be considered. For

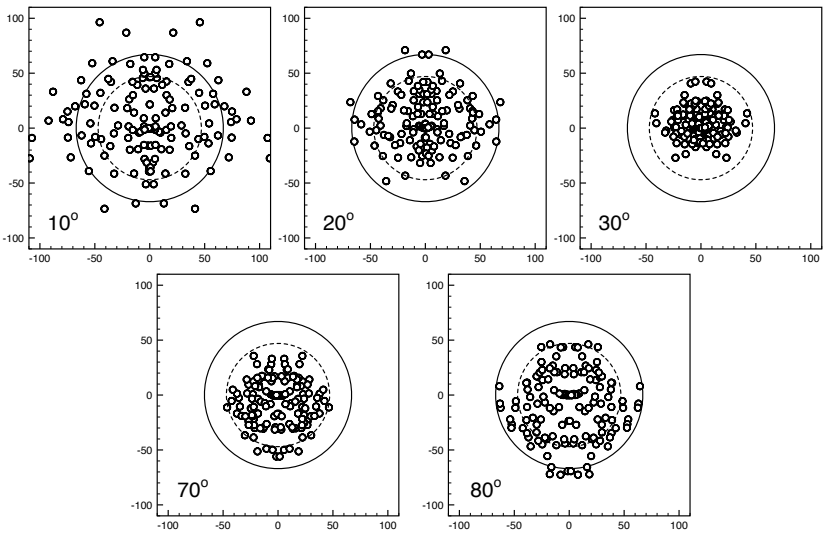

Fig. 8. Focus maps at the receiver entrance for five sun elevations [15]. Solid circle: geometrical CR of 2000. Dashed circle: target to avoid spillage caused by finite sun size. Each dot indicates a ray reflected from a corner or the center of one of the 32 reflectors used for calculation.

example, it may be more cost-effective to approximate the ideal nearly-paraboloidal surface shape with sections of spheres of a small number of different radii, blurring the focus a little further than shown in Fig. 8.

If the ideal size of the PWF 'segmented dish' is an order of magnitude larger than for a conventional paraboloidal dish (see discussion in [14]), e.g. 5000 m^2, then 250 reflectors would have an area of 20 m^2 each, which is well within the range of sizes for current heliostat designs [16] and likely to be quite economical to produce. At 5000 m^2 aperture area the aperture radius and maximum rim height would both be about 40 m, and average thermal output would be about 4 MW.

6 Receiver design for PWF collectors

The assessment of collector optical performance in the sections above depended on the size and shape of the receiver to be used, and as noted, a big advantage of the PWF concept is that its converging cone of reflected light is suitable for a cavity receiver. Efficiency of a cavity receiver is likely to be considerably higher than that of an open cylindrical receiver as used for Gen 2 CST (see below). A true cavity receiver has a small opening through which concentrated sunlight passes and then fans out to heat a much larger internal area of absorber surface, of order ten times larger than the opening (or more). If the exterior is well insulated, heat is lost only from the opening, by blackbody radiation and by mixed convection (passive and wind-driven).

As noted by Mehos et al [1], Sedighi et al [17], and others, compressed gases have many advantages as the heat transfer fluid from absorber to heat store. Various common gases are non-toxic, non-flammable, inexpensive, non-condensing and non-freezing, and they allow fast startup after sunrise. Compressed gases have the further advantage over molten salt of simplicity of operation in a distributed network of pipes serving multiple PWF collectors, since trace heating is not required and thermal inertia is low. The big disadvantage of compressed gases is their low forced-convection heat transfer coefficients. However, heat transfer to a gas can be improved by a combination of (a) large temperature differential from the walls of the absorber, (b) high system pressure to increase gas density, (c) high gas velocity (limited by pumping power losses), and (d)

Table 1. Possible absorber designs using CO_2 in standard sizes of 316 stainless steel tube

Concentration ratio at absorber	100	200	100	200	200
HTF pressure, bar	100	100	200	200	200
Tube outside diameter, mm	22.2	22.2	15.9	15.9	9.52
Wall thickness, mm	1.2	1.2	1.6	1.6	0.9
Hoop stress, MPa	82.5	82.5	79.4	79.4	86
ΔT through wall, K	4.5	9	6	12	6.7
ΔT convection, K	77	88	48	55	49
Number of tubes per m^2 of absorber, and length, m	2@20	2@20	3@16.7	3@16.7	8@11.4
Circulation power, W/m^2, (as % of shaft power)	50 (0.17%)	348 (0.6%)	40 (0.13%)	280 (0.47%)	358 (0.6%)
Mass of steel per 1.0 m^2 of *receiver aperture*, kg	496	248	560	280	173

large absorber area. For a steam-Rankine power block with inlet temperature 565 C and heat store (molten salt) at 585 C, the required gas temperature at the receiver outlet will be around 620 C. The absorber surface could be roughly 70 C hotter (inferred from Table 1) at an absorber concentration ratio of 200, peaking at 690 C. At a CR of 900 (typical of cylindrical receivers, e.g. [7]) a similar absorber surface would peak at 935 C, probably not feasible at reasonable cost with currently available metal alloys. By separating the absorber area from the heat loss area (the cavity opening), the heat losses can be made quite small while the absorber area is large enough to handle heat transfer to a compressed gas.

Kim, Kim and Stein [18] made a detailed CFD study of heat loss from several receivers, including an open panel (equivalent to a cylindrical power tower receiver) and a cavity receiver with entrance area 1/20th of the size of the absorber area. Their efficiency results for the open panel at 530 C compared very well with the experimental results for Solar Two [19], indicating peak efficiency of 84% to 89%. At 600 C surface temperature, 5 m/s wind speed, 6% reflectivity from the Pyromark surface, and 300 or 600 kW/m^2 incident sunlight, open panel receiver efficiency is 80% or 87% respectively. Under similar conditions except for 80 kW/m^2 on the absorber area (corresponding to a PWF collector with CR of 2000 at the cavity entrance), the cavity receiver efficiency is 96%, using the relevant Kim, Kim and Stein [18] heat loss results. For comparison, the cavity receiver of the ANU SG4 paraboloidal dish has a CR of 2240, and it achieves over 97% efficiency generating steam at 510-560 C [20]. Thus the cavity receiver not only facilitates the use of a compressed gas heat transfer fluid, it also gains efficiency quite significantly compared to a Gen 2 molten salt receiver.

Several compressed gases were studied as potential heat transfer fluids (HTF), and various gas mixtures also show promise, but the aim in this section is to show that the assumed absorber conditions are feasible with readily available, moderate-cost materials, namely compressed CO_2 and standard sizes of 316 stainless steel tubing [21]. The design concept

is that the illuminated wall areas of the cavity are lined with a number of tubes carrying the gas in parallel, with small gaps between them, and following roughly helical paths. Connection to some form of inlet and outlet manifolds will be a crucial design detail, not considered here. Sunlight flux density entering the receiver was taken as 1600 kW/m^2 and thus 80 or 160 kW/m^2 at the absorber. Steel properties used [22] were conductivity 21.4 W/(m·K) and yield stress (at 650 C) 145 MPa; however, rupture stress after 100K hours at 650 C is 94 MPa. Unknown levels of stress caused by thermal gradients and absorber mountings will need to be added to the calculated hoop stresses. The heated area for ΔT calculation was taken conservatively as tube length times tube spacing (instead of half the circumferential area). Inlet and outlet temperatures were 320 C and 620 C, and CO_2 properties were evaluated at 500 C only (these calculations are a first approximation). The Dittus-Boelter equation [23] was used for Nusselt number, and the Petukhov friction factor equation [23] was used for pressure drop along the tube.

Some results are given in Table 1, using two values of system pressure and two values of CR at the absorber. The percentage values for circulation power consumption (parasitic power) are relative to the assumed power block outputs of 30 kW_e from 80 kW/m^2 input and 60 kW_e from 160 kW/m^2. These percentages do not include circulation power consumption in the pipework connecting receivers to thermal storage, and in the CO_2-salt heat exchanger.

Ideally, temperature differences, circulation power, mass of steel, and complexity (the number of tubes in parallel), would all be kept very low, but in practice there are compromises. Taking the design in column 1 as a base case, increasing the CR (column 2) halves the mass of steel but increases both peak temperature and parasitic power. Increasing the CO_2 pressure (column 3) reduces peak temperature but requires even more steel than in the base case. Combining higher CR and pressure (column 4) gives the best results, subject to further optimization. The design in the last column reduces the mass of steel even further and has smaller temperature differences, at the expense of much greater complexity. In any case, it is clear that a workable high-efficiency cavity receiver can be designed. Also, peak temperature in the tubing can be reduced by using non-uniform sunlight flux density onto the absorber. Another design possibility is to use an absorber based on compact heat exchanger technology [24]. Detailed thermal modelling of cavity receivers will be incorporated into NREL's System Advisor Model (SAM) software [25], which may facilitate the design of the absorber, especially when the PWF collector is not radially symmetrical.

7 Discussion

The analysis so far has shown the technical feasibility of PWF collectors, so the next step is to consider how their use would affect the cost of a CST power plant. In a Gen 2 power tower plant with a solar multiple of 2.1, the heliostats and receiver made up nearly 60% of the total cost [26], so there is scope for significant cost reduction if they can be replaced effectively. This can be achieved by reducing the area of reflector required through increased efficiency, and by reducing the cost per m^2 of reflector. Some aspects of collector efficiency are set out in Table 2 in terms of their effect on the area of PWF reflectors relative to heliostat area. Other aspects such as mirror reflectance and cleanliness are likely to be very similar for the two technologies. The most important benefit stems from the way the PWF reflectors are comparatively 'square-on' to the sun throughout the day, leading to a better average cosine factor, but the cavity receiver benefits are also important. Note that about two hours elapse after sunrise before a molten salt power tower reaches stable operation [19], whereas the PWF collectors can be brought into operation quite quickly. The product of the five area ratios in the table is 0.62, i.e. the area of

Table 2. Efficiency factors reducing PWF mirror area relative to power tower heliostat area

	Power tower	**PWF**	**Relative area**
Cosine factor	0.71	0.9	0.79
Dispersion	0.97	1.0	0.97
Receiver absorption	0.94	1.0	0.94
Heat retained [1.0 − heat loss]	0.9	0.96	0.94
Hours of operation	0.89	0.98	0.91
Combined relative area			**0.62**

reflectors in PWF collectors will be about 62% of the power tower heliostat total area for equal heat collection.

Comparative costing of a PWF collector per m^2 of reflector is not easy at this stage, but some influential factors are noted here. The reflector surface itself is similar to that of a heliostat, but the heliostat pedestal and two-axis precision gear drives can be replaced by simple bearing mounts and one linear actuator. The eliminated gear drives, pedestal and its foundation comprise about 50% of the cost of a large conventional heliostat (Table 3-14 in [13]). On the other hand, the rotating base frame is a necessary new element, but this can be a lightweight steel space-frame anchored to a central pivot point and travelling on a simple horizontal track; it is unlikely to be very expensive per m^2 of reflector. For the cavity receiver, the absorber will be around three times larger in area and require external insulation, but the receiver will not need any of the ancillary reservoirs, drain-back system or trace heating needed for a molten-salt central receiver. Thus the total cost of a PWF collector per m^2 of reflector is likely to be comparable to (but not greater than) that of a central receiver with heliostat surround field. The most significant saving in the cost of a CST power plant arises from from the much smaller area ratio (around 62%).

The fast-start benefit of a compressed-gas receiver was mentioned above, but there are other operational advantages too. Cylindrical central receivers in a surround field of heliostats are heated differentially throughout the day — hotter on the western side in the morning, and on the eastern side in the afternoon — whereas PWF collectors rotate to follow the sun. Also, variable cloud cover over part(s) of the heliostat field results in highly uneven heating of the central receiver, making stable operation difficult or impossible [19]. Multiple PWF collectors will be required for a power station of more than a few MW, so those that are not directly affected by a cloud transient will continue normal operation, and the gaseous HTF allows affected collectors to recover quickly. Note also that PWF collectors operating at higher temperatures could be used to charge solid particle thermal storage instead of molten salt, informed by designs for particle-to-sCO_2 heat exchangers [6] but working in reverse (sCO_2-to-particle heat transfer).

In the ten years since the Gen 2 CST cost reduction study [26] the cost of photovoltaic (PV) panels has dropped most remarkably, and hundreds of GW of PV panels have been deployed in many regions at both rooftop and utility scale. This has led to the so-called ‘duck curve’ of electricity spot prices, where the price is depressed around the middle of the day but rises rapidly in the late afternoon. Using the Australian National Energy Market as an example, the twelve-month average

spot price per MWh for 2019-2020 was A$25 to A$50 for several hours around midday, and rose to about A$180 at 6 pm (Fig. 1.3 of [27]). CST power plants with storage are well-placed to supply electricity in such situations when demand and prices are high, and in an extreme case the power block would operate for only a few hours per day. The solar multiple would be less than 1.0, reducing the total cost of plant per MW but de-emphasising the proportional cost of the collectors. However, CST base-load power plants may have a future role as coal-burning power plants are retired, and the power blocks will be designed for continuous rather than intermittent operation. The solar multiple will be nearer 3.0, increasing the value of lower cost, high performance collector fields such as PWF designs. Requirements for island grids and remote sites are similar.

Note: This research did not receive any funding from public, not-for-profit, or commercial agencies.

References

[1] Mehos, M., Turchi, C., Vidal, J., Wagner, M., Ma, Z., Ho, C., Kolb, W., Andraka, C., Kruizenga, A., 2017. *Concentrating Solar Power Gen3 Demonstration Roadmap,* National Renewable Energy Laboratory, Golden CO, NREL/TP-5500-67464

[2] National Renewable Energy Laboratory, 2021. *Concentrating Solar Power Projects: Solana Generating Station CSP Project*, Status Date: December 5, 2021, National Renewable Energy Laboratory, Golden CO. https://solarpaces.nrel.gov/project/solana-generating-station

[3] Relloso, S., Gutierrez, Y., 2017."SENER molten salt tower technology. Ouarzazate NOOR III case," AIP Conference Proceedings **1850**, p. 030041. https://doi.org/10.1063/1.4984384

[4] Ho, C. K., Christian, J. M., Yellowhair, J. E., Armijo, K., Kolb, W. J., Jeter, S., Golob, M., and Nguyen, C., 2019. "On-Sun Performance Evaluation of Alternative High-Temperature Falling Particle Receiver Designs," ASME J. Sol. Energy Eng., **141**(1), p. 011009. https://doi.org/10.1115/1.4041100

[5] Gonzalez-Portillo, L. F., Albrecht, K. J., Sment, J., Mills, B., Ho, C. K., 2022. "Sensitivity Analysis of the Levelized Cost of Electricity for a Particle-Based Concentrating Solar Power System", ASME J. Sol. Energy Eng., **144**(3), p. 031002. https://doi.org/10.1115/1.4053167

[6] Ho, C. K., Carlson, M., Albrecht, K. J., Ma, Z., Jeter, S., Nguyen, C. M., 2019. "Evaluation of Alternative Designs for a High Temperature Particle-to-sCO_2 Heat Exchanger", ASME J. Sol. Energy Eng., **141**(2), p. 021001. https://doi.org/10.1115/1.4042225

[7] Dunham, M. & Iverson, B., 2014. "High-efficiency thermodynamic power cycles for concentrated solar power systems," Renewable and Sustainable Energy Reviews **30**(C), pp. 758-770 https://doi.org/10.1016/j.rser.2013.11.010

[8] Falcone, P., 1986. *A Handbook for Solar Central Receiver Design,* Sandia National Laboratories, Livermore CA, SAND 86-8009

[9] Baum, V., Aparasi, R., Garf, B., 1957. "High-power solar installations," Solar Energy **1**(1), pp. 6-12

[10] Li, L., Coventry, J., Bader, R., Pye, J., Lipiński, W., 2016. "Optics of solar central receiver systems: a review," Optics Express **24**(14), pp. A985-A1007 https://doi.org/10.1364/OE.24.00A985

[11] Jones, D., 1982. "Heliostatic solar energy conversion system," Patent US4365618

[12] Ruiz, V., Frasquet, M., Martínez, F., Silva, M., Lillo, I., Díaz Andrades, F., Lobo Márquez, G., 2014. "The variable geometry central receiver system concept. First results and comparison with conventional central receiver systems," Energy Procedia **57**, pp. 2255-2264 https://doi.org/10.1016/j.egypro.2014.10.233

[13] Kolb, G., Jones, S., Donnelly, M., Gorman, D., Thomas, R., Davenport, R., Lumia, R., 2007. *Heliostat Cost Reduction Study,* Sandia National Laboratories, Albuquerque NM, SAND2007-3293

[14] Bisset, D., 2016. "Testing the 'Segmented Dish' Piecewise-Focusing Solar Collector," in: Proc Asia Pacific Solar Research Conference 2016, Australian PV Institute, Redfern NSW, ISBN: 978-0-6480414-0-5 https://doi.org/10.5281/zenodo.6131584.

[15] Bisset, D., 2017. "Images Formed by a Piecewise-Focusing Solar Collector," in: Proc Asia Pacific Solar Research Conference 2017, Australian PV Institute, Redfern NSW, ISBN:978-0-6480414-1-2 https://doi.org/10.5281/zenodo.6131613

[16] Coventry, J., Pye, J., 2014. "Heliostat cost reduction — where to now?" Presented at SolarPACES 2013, Energy Procedia **49**, pp. 60-70 https://doi.org/10.1016/j.egypro.2014.03.007

[17] Sedighi, M., Padilla, R., Taylor., R, Lake, M., Izadgoshasb, I., Rose, A., 2019. "High-temperature, point-focus, pressurised gas-phase solar receivers: A comprehensive review," Energy Conversion and Management **185**, pp. 678-717 https://doi.org/10.1016/j.enconman.2019.02.020

[18] Kim, J., Kim, J.-S., Stein, W., 2015. "Simplified heat loss model for central tower solar receiver," Solar Energy **116**, pp. 314-322 https://doi.org/10.1016/j.solener.2015.02.022

[19] Pacheco, J. (ed), 2002. *Final Test and Evaluation Results from the Solar Two Project,* Sandia National Laboratories, Albuquerque NM, SAND2002-0120

[20] Pye, J., Coventry, J., Venn, F., Zapata, J., Abbasi, E., Asselineau, C.-A., Burgess, G., Hughes, G., Logie, W., 2017. "Experimental testing of a high-flux cavity receiver," SolarPACES 2016, AIP Conference Proceedings **1850**, 110011, https://doi.org/10.1063/1.4984485

[21] Atlas Steels, 2020. *Atlas Steels Product Reference Manual (July 2020)*, Atlas Steels, Melbourne, Australia. https://atlassteels.com.au/wp-content/uploads/2021/08/Atlas-Steels-Product-Manual-Section-4.pdf

[22] American Society for Metals Handbook Committee, 1989. *Metals Handbook,* 9th ed., American Society for Metals, Metals Park OH

[23] Incropera, F., DeWitt, D., 1996. *Fundamentals of Heat and Mass Transfer (4th ed),* John Wiley & Sons, New York

[24] Besarati, S. M., Goswami, D. Y., Stefanakos, E. K., 2015. "Development of a Solar Receiver Based on Compact Heat Exchanger Technology for Supercritical Carbon Dioxide Power Cycles", ASME J. Sol. Energy Eng., **137**(3), p. 031018. https://doi.org/10.1115/1.4029861

[25] Kerkhoff, J. A., Wagner, M. J., 2021. "A Flexible Thermal Model for Solar Cavity Receivers Using Analytical View Factors", ASME 15th International Conference on Energy Sustainability, Paper ES2021-63810, ISBN 978-0-7918-8488-1. https://doi.org/10.1115/ES2021-63810

[26] Kolb, G., Ho, C., Mancini, T., Gary, J., 2011. *Power Tower Technology Roadmap and Cost Reduction Plan,* Sandia National Laboratories, Albuquerque NM, SAND2011-2419

[27] Australian Energy Regulator, 2020. *Wholesale Markets Quarterly, Q2 2020*, Australian Energy Regulator, Melbourne.

